Time-Resolved Seismic Tomography Detects Magma Intrusions at Mount Etna

D. Patanè, *et al.*

Science **313**, 821 (2006);
DOI: 10.1126/science.1127724

Time-Resolved Seismic Tomography Detects Magma Intrusions at Mount Etna

D. Patanè,[1]* G. Barberi,[1] O. Cocina,[1] P. De Gori,[2] C. Chiarabba[2]

The continuous volcanic and seismic activity at Mount Etna makes this volcano an important laboratory for seismological and geophysical studies. We used repeated three-dimensional tomography to detect variations in elastic parameters during different volcanic cycles, before and during the October 2002–January 2003 flank eruption. Well-defined anomalous low *P*- to *S*-wave velocity ratio volumes were revealed. Absent during the pre-eruptive period, the anomalies trace the intrusion of volatile-rich (≥4 weight percent) basaltic magma, most of which rose up only a few months before the onset of eruption. The observed time changes of velocity anomalies suggest that four-dimensional tomography provides a basis for more efficient volcano monitoring and short- and midterm eruption forecasting of explosive activity.

Repeated seismic tomography [four-dimensional (4D) tomography: in space and time] can be used to reveal variations of elastic properties within rock volumes. This approach has been used in geothermal and volcanic areas (*1*, *2*) and in hydrocarbon surveillance (*3*), in order to monitor gas concentration and migration and to track changes during exploitation, respectively. Seismic velocity variations depend on the characteristics of the rock (such as mineralogy, porosity, fracturing, and fluid saturation) and its physical conditions (such as temperature and pressure) (*4*–*7*). In a volcanic environment, the presence of fluids, cracks, and gas, or their temporal variations within the plumbing system, may also change the elastic properties drastically and suddenly (*8*–*10*).

Mount Etna, a basaltic stratovolcano located near a densely populated area, is commonly considered to exhibit only effusive eruptions. However, it is one of the few alkali-basaltic volcanoes for which several violent explosive (subplinian and plinian basaltic-type) eruptions are documented (*11*). Recently, from 27 October 2002 to 18 January 2003, a flank eruption (Fig. 1) was characterized by an intense explosive activity with column-forming fire fountains and fairly continuous tephra fallout. This peculiar activity was fed by the uprising of a new intrusion of volatile-rich basaltic magma, containing CO_2-rich gas of deep derivation (>10 km) (*12*, *13*). Because repeated seismic tomography may be a reliable indicator of the migration of fluids in active volcanoes (*2*), this approach may allow the detection of the transient presence of magmatic intrusions that are rich in gas and provide a valuable tool for future forecasting of Mount Etna's volcanic activity. However, some problems may arise when a tomographic study is applied to evaluate the temporal variations of elastic parameters, because the resolution of velocity models may differ by inverting contiguous short-period data sets. Moreover, the dimension of resolvable features may be higher than that of rapidly changing local anomalies, and normally we lack independent evidence for physical phenomena that change elastic parameters over time. Conversely, if a long-period data set is used in the tomographic analysis, the spatial distribution of the anomalies may be biased or obscured by averaged values when the volcano is characterized by highly eruptive dynamics.

In our study, the use of a large number of permanent seismic stations and the abundance of local earthquakes, occurring both before and during the eruptions, guarantee a consistent and high-resolution velocity model. We analyzed the seismicity (Fig. 2) recorded at the Mount Etna Istituto Nazionale di Geofisica e Vulcanologia–Sezione di Catania (INGV-CT) computerized permanent seismic network (Fig. 1) before and during the 2002–2003 flank eruption. The permanent network was composed of 45 stations, 5 of which were three-component short-period (1 s) stations and three of which were digital three-component broad-band (40 s) stations. On 6 November 2002, a temporary array composed of eight digital three-component broad-band (60 s) stations was integrated into the permanent network in the northern sector

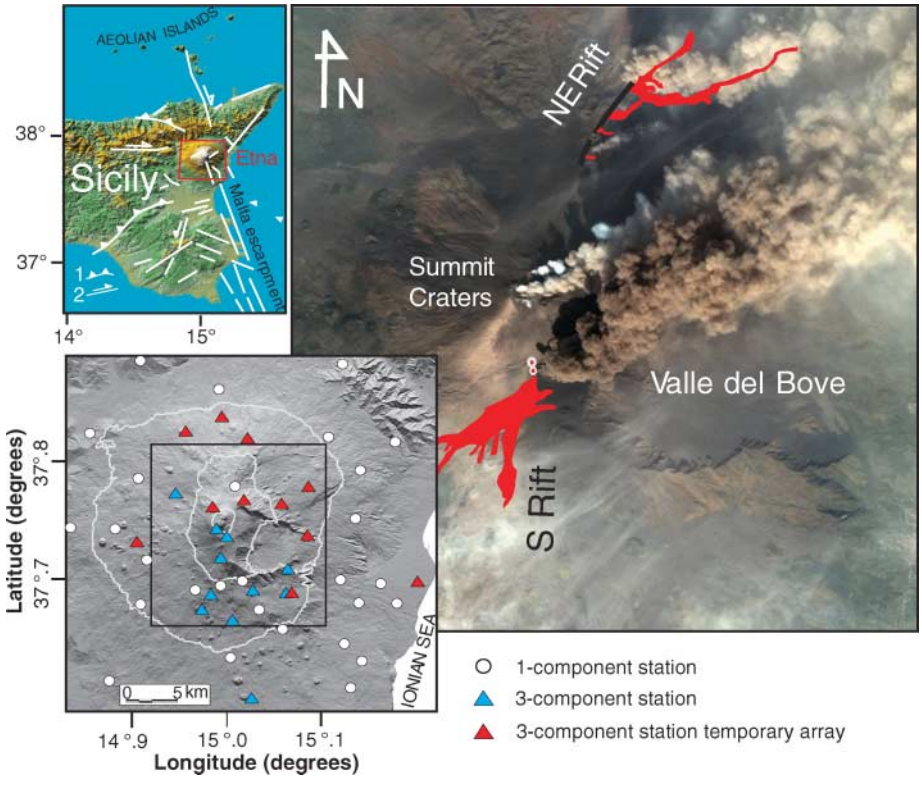

Fig. 1. (**Right**) Image of the summit of the Mount Etna volcano showing the ash plumes during one day of the 27 October 2002 to 18 January 2003 eruption [image acquired by Digital Globe's Quickbind-2 satellite (http://rst.gsfc.nasa.gov/Sect13/Sect13_4d.html)]. Eruptive fissures opened on the northeast and south rifts of the volcano. Black lines, eruptive fractures; red areas, lava flows. (**Top left**) Structural map of eastern Sicily showing the front of the Appenninic-Maghrebian chain (1) and the main faults (2). (**Bottom left**) Map of the Mount Etna area indicating the seismic stations operating during the study period. The black square indicates the summit of the volcano shown in the image on the right. The concentric white curves represent elevation contours at 1000-m intervals.

[1]Istituto Nazionale di Geofisica e Vulcanologia, Sezione di Catania, Piazza Roma, 2, 95123, Catania, Italy. [2]Istituto Nazionale di Geofisica e Vulcanologia, Centro Nazionale Terremoti, Via di Vigna Murata, 605, 00143, Roma, Italy.

*To whom correspondence should be addressed. E-mail: patane@ct.ingv.it

of the volcano. During the study period, some stations were moved, depending on the location of seismicity.

First, we performed a tomographic inversion of the whole data set (10 August 2001 to 18 January 2003) to define the 3D *P*-wave velocity (V_P) and the structure of the *P*- to *S*-wave velocity ratio (V_P/V_S). A total of 712 well-constrained earthquakes [root mean square (rms) time residuals ≤0.2 s; horizontal (Erh) and vertical (Erz) hypocentral location errors ≤1.0 km; azimuthal gap of the stations ≤120°], 8587 *P*-wave arrivals, and 2293 *S*-wave arrivals were inverted to model a grid 2 km by 2 km by 1 km with the use of SIMULPS-14 software (*14*). On the digital seismograms, the measured time pickings were precise to ~0.01 s, and phase arrivals were checked by polarization analysis, especially for the *S* waves. The starting velocity model was derived from the 3D model developed by Patanè *et al.* (*15*). The input value for the V_P/V_S ratio was 1.73, which is in agreement with the results of Laigle (*16*). After 10 iterations, the variance improvement was 34.7%, with a final rms value of 0.20 s (table S1). The reliability of the V_P and V_P/V_S models has been verified by the analyses of the full-resolution matrix (Fig. 3) and by synthetic tests [supporting online material (SOM) text]. This inversion allows the improvement of even the most recent tomographic results (*15*, *17*) and better definition of the shape and geometry of the upper portion of high-velocity V_P volume, interpreted as a main solidified intrusive body (*15*) (Fig. 3A). However, the most notable result concerns the detection of anomalous zones with low V_P/V_S values (*18*).

The V_P/V_S images, which present a satisfactory resolution [spread function (SF) ≤2] between the depths of –4 and 2 km (Fig. 3B), clearly highlighted two anomalous regions characterized by low V_P/V_S values (as small as 1.64). These were located in the central-southern and northeastern part of the volcanic edifice, where geodetic data modeled the dike intrusions of 2002–2003 (*19*, *20*) (Fig. 3B) and beneath the eruptive fracture systems (Fig. 1).

Because the V_P/V_S ratio can be very sensitive to factors that may change with time during the magmatic cycles, we separately analyzed the pre-eruptive (10 August 2001 to 25 October 2002) and the eruptive (26 October 2002 to 18 January 2003) seismicity. We further subdivided the pre-eruptive period into two time intervals because geochemical observations, ground deformation measurements obtained via Global Positioning System (GPS) technology, and seismicity evidence (Fig. 2C) (*20*) indicated that there was a recharging phase, which started in April

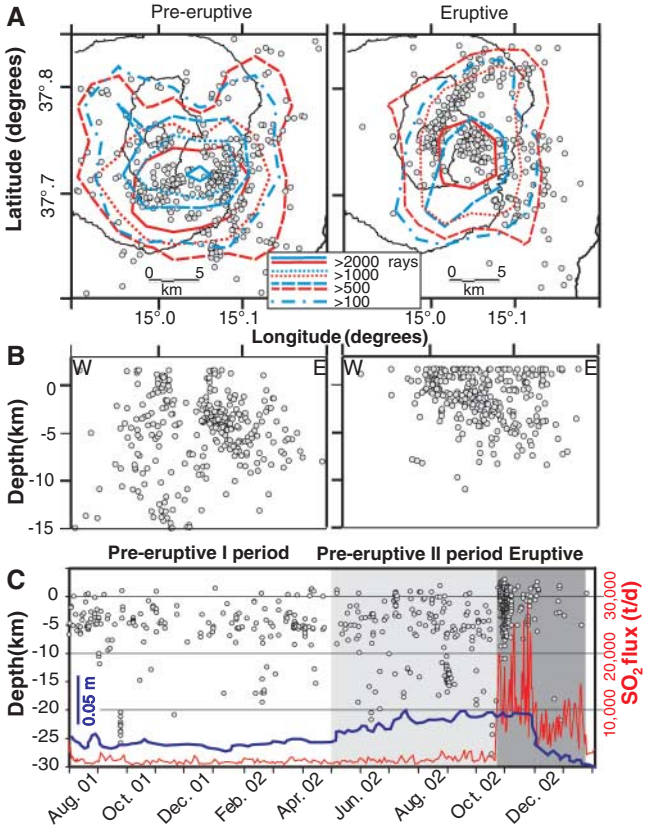

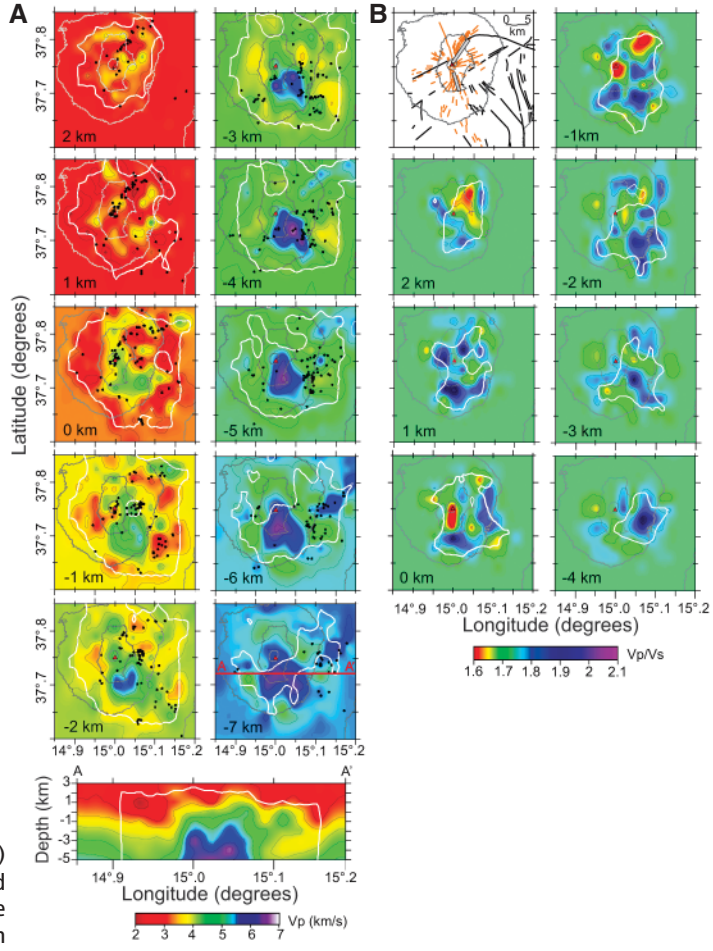

Fig. 2. (**Left**) Maps of (**A**) 1D epicentral locations (gray circles) and (**B**) related W-E cross sections across the summit craters for 712 selected earthquakes that were recorded during the pre-eruptive and eruptive periods. In (A), the sum of the rays contributing to the solution at each grid node that was defined for the inversion is represented by the density contours for both *P* (red lines) and *S* waves (blue lines). (**C**) The plot versus time of focal depths for the whole data set (gray circles), ground deformation time series related to a central-western GPS baseline (*20*) (blue line), and SO_2 flux daily measurements (red line). t/d, metric tons per day. Note (i) the increasing rate of ground deformation since April 2002 (light gray area); (ii) the slight increase in SO_2 flux since August; and (iii) the very high value of SO_2 flux (up to ~30,000 t/d) measured during the eruptive period (dark gray area). **Fig. 3.** (**Right**) Velocity models for V_P (**A**) and V_P/V_S (**B**) in the well-resolved layers. The white contours indicate the regions of the model with SF values <2 and where the resolution is good (SOM text) (*27*, *28*). The gray lines are elevation isolines (every 1000 m). The black dots in the Vp model (A) are the earthquakes relocated with the 3D velocity model. The W-E cross section of the V_P model crossing the grid center (red horizontal line) is reported in the –7-km layer. In the top left square of (B), historical eruptive fissures (orange lines), major faults (black lines), and the surface projection of the 2002–2003 dike intrusions (gray rectangles) modeled by geodetic data (*19*, *20*) are shown.

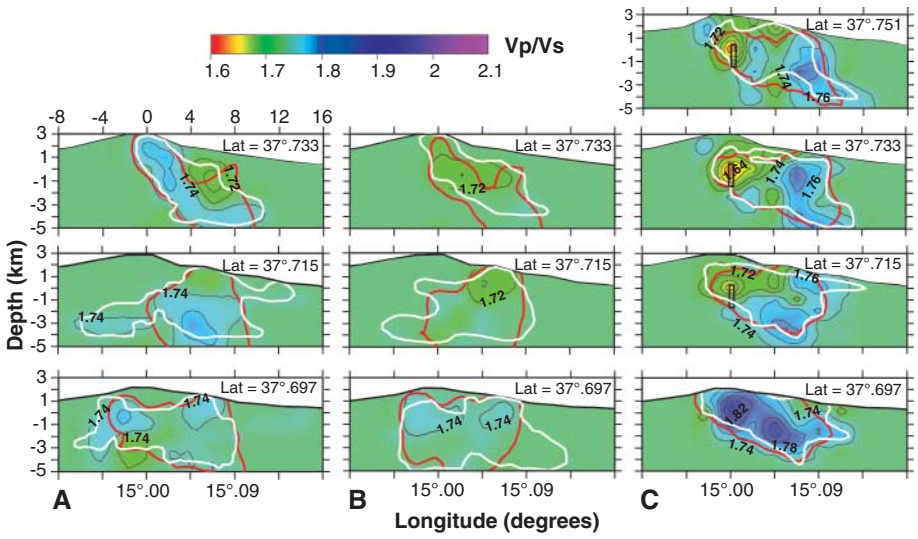

Fig. 4. W-E cross sections showing the variation of the V_P/V_S ratio during the pre-eruptive periods [(**A**) and (**B**)] and the 2002–2003 eruption (**C**). The vertical black rectangle in (C) indicates the location of the 2002–2003 dike intrusion, as modeled by geodetic data in the southern flank (*19*, *20*). The white and red lines indicate the well-resolved regions of the model with SF values <2 and derivative weight sum values >50, respectively (SOM text).

2002, following an approximate 8-month period of deflation at the end of the 2001 flank eruption.

For these inversions and for each epoch, we verified the reliability of the V_P/V_S models (SOM text) as described above, by using both the analyses of the full-resolution matrix (Fig. 4 and fig. S1) and synthetic tests (fig. S2). In west-to-east (W-E) cross sections for the different analyzed periods (Fig. 4), we observed a substantial change of V_P/V_S anomalies through time. During the 2002–2003 eruption, strong anomalies with low V_P/V_S values were revealed beneath the central-southern and northeastern parts of the volcanic edifice. Conversely, high or normal V_P/V_S values were found in the same region during the deflation after the end of the 2001 eruption (Fig. 4A) and the pre-eruptive recharging period (Fig. 4B). The time change of V_P/V_S anomalies revealed a variation of both fluid and fluid pressure in the shallow layers (depth <5 km), due to the uprising of magma from greater depth that started only a few months before the onset of the 2002–2003 eruption (*13*, *21*).

Geochemical and petrological features of the erupted lavas (*13*, *22*), and evidence for the expulsion of a large volume of pyroclastic products [40×10^6 m^3 to 50×10^6 m^3 with an explosive index of ~0.55 (*22*)] during the eruption, support the hypothesis that these low V_P/V_S volumes are related to the intrusion of volatile-rich [≥4 weight % (*12*, *13*)] basaltic magma.

During the eruptive period, we observed wide regions with high V_P/V_S anomalies mainly located beneath the eastern and southeastern flanks of the volcano (Fig. 4C). It is widely accepted that melt-filled inclusions result in a high V_P/V_S ratio (*8*–*10*), even if the effects of a partial melt on seismic wave velocities are still poorly known. However, the possibility of a partial melt cannot be entirely excluded from having occurred inside the regions of high V_P/V_S values, especially near the central craters and southward where the magma intruded during 2001 (*23*). We hypothesize that the high V_P/V_S anomalies are related to the rapid migration of fluids from the intrusion zone into the fractured regions beneath the eastern and southeastern flanks (*24*). In these regions, crack density increases because of the intense fracturing occurring both during the pre-eruptive and eruptive periods (see the location of seismicity in Fig. 2).

On the basis of the geophysical evidence presented here, we believe that the extensive application of 4D tomography could be widely used in volcanic monitoring and in the prediction of violent explosive eruptions generated by gas-rich magma. However, this technique requires high-quality, densely positioned, three-component seismic networks, which were not available during previous large eruptions at Mount Etna and are not in place at most volcanoes worldwide.

References and Notes

1. B. R. Julian, A. M. Pitt, G. R. Foulger, *Geophys. J. Int.* **133**, F7 (1998).
2. G. R. Foulger *et al.*, *J. Geophys. Res.* **108**, 10.1029/2000JB000041 (2003).
3. G. Guerin, W. He, R. N. Anderson, L. Xu, U. T. Mello, in *2000 Offshore Technology Conference*, paper 12101, www.ces-enterprise.com/vpatch/bp/attachments/OTC2000_Guerin.pdf.
4. R. O'Connell, B. Budiansky, *J. Geophys. Res.* **79**, 5412 (1974).
5. N. I. Christensen, W. W. Wepfer, *Geol. Soc. Am. Mem.* **172**, 91 (1989).
6. Z. W. Wang, A. Nur, *Soc. Pet. Eng. Res. Eng.* **3**, 429 (1989).
7. J. Dvorkin, G. Mavko, A. Nur, *Geophys. Res. Lett.* **26**, 3417 (1999).
8. G. Mavko, *J. Geophys. Res.* **85**, 5173 (1980).
9. H. Sato, I. S. Sacks, T. Murase, *J. Geophys. Res.* **94**, 5689 (1989).
10. C. O. Sanders, S. C. Ponko, L. D. Nixon, E. A. Schwartz, *J. Geophys. Res.* **100**, 8311 (1995).
11. M. Coltelli, P. Del Carlo, L. Vezzoli, *Int. J. Earth Sci.* **89**, 665 (2000).
12. R. Clocchiatti, M. Condomines, N. Guenot, J. C. Tanguy, *Earth Planet. Sci. Lett.* **226**, 397 (2004).
13. N. Spilliaert, P. Allard, N. Métrich, A. V. Sobolev, *J. Geophys. Res.* **111**, 10.1029/2005JB003934 (2006).
14. C. H. Thurber, in *Seismic Tomography: Theory and Practice*, H. M. Iyer, K. Hirahara, Eds. (Chapman and Hall, London, 1993), pp. 563–583.
15. D. Patanè, C. Chiarabba, P. De Gori, A. Bonaccorso, *Science* **299**, 2061 (2003).
16. M. Laigle, A. Hirn, M. Sapin, J. C. Lepine, *J. Geophys. Res.* **105**, 21,633 (2000).
17. C. Chiarabba, P. De Gori, D. Patanè, in *Mt. Etna: Volcano Laboratory*, A. Bonaccorso, S. Calvari, M. Coltelli, C. Del Negro, S. Falsaperla, Eds. (Geophysical Monograph Series, American Geophysical Union, Washington, DC, 2004), pp. 191–204.
18. For igneous rocks, laboratory experiments found that the V_P/V_S ratio generally decreases as temperature increases and increases as pressure increases. An increase in the V_P/V_S ratio is related to increases in temperature, fracture, and especially partial melt, whereas a decrease in the ratio can be associated with the presence of gas or supercritical fluids [see (*10*) and references therein].
19. M. Aloisi, A. Bonaccorso, S. Gambino, M. Mattia, G. Puglisi, *Geophys. Res. Lett.* **30**, 10.1029/2003GL018896 (2003).
20. D. Patanè, M. Mattia, M. Aloisi, *Geophys. Res. Lett.* **32**, 10.1029/2004GL021773 (2005).
21. S. Gambino, A. Mostaccio, D. Patanè, L. Scarfì, A. Ursino, *Geophys. Res. Lett.* **31**, 10.1029/2004GL020499 (2004).
22. D. Andronico *et al.*, *Bull. Volcanol.* **67**, 10.1007/s00445-004-0372-8 (2005).
23. C. Martínez-Arevalo, D. Patanè, A. Rietbrock, J. Ibanez, *Geophys. Res. Lett.* **32**, 10.1029/2005GL023736 (2005).
24. Theory predicts that the velocity decreases and V_P/V_S increases for increasing crack density (*4*). High V_P/V_S values affecting portions of fault zones, such as at the San Andreas Fault, are interpreted as evidence for the presence of overpressured fluids (*25*). The influence of pore pressure on seismic velocities is caused by the tendency of cracks to remain open when they are internally pressurized (*26*). Thus, fracturing and increasing pore pressure cause a relatively marked decrease of V_S but only a small decrease of V_P, which yields an increased V_P/V_S ratio. The concentration of fluids in a dike intrusion mainly occurs near its tip. Moreover, a rapid migration of fluids in the surrounding rock volume can also occur, especially when prefractured zones exist, leading to a high V_P/V_S ratio and to an increase of the seismicity (Figs. 2 and 4C).
25. C. H. Thurber *et al.*, *Geophys. Res. Lett.* **24**, 1591 (1997).
26. A. Nur, *Bull. Seismol. Soc. Am.* **62**, 1217 (1972).
27. A. Michelini, T. V. McEvilly, *Bull. Seismol. Soc. Am.* **81**, 524 (1991).
28. M. Reyners, D. Eberhart-Phillips, G. Stuart, *Geophys. J. Int.* **137**, 873 (1999).

29. We thank T. Caltabiano for SO_2 flux data and anonymous referees for helpful comments and suggestions on the manuscript. This work was supported by grants from the European Union VOLUME FP6-2004-Global-3 and INGV–Department of Civil Protection V3/6 projects.

Supporting Online Material

www.sciencemag.org/cgi/content/full/313/5788/821/DC1
SOM Text
Figs. S1 and S2
Table S1

21 March 2006; accepted 29 June 2006
10.1126/science.1127724